This article has been accepted for inclusion in a future issue of this journal. Content is final as presented, with the exception of pagination.

Lane-Level Integrity Provision for Navigation and Map Matching With GNSS, Dead Reckoning, and Enhanced Maps

Rafael Toledo-Moreo, *Member, IEEE*, David Bétaille, *Associate Member, IEEE*, and François Peyret

***Abstract*—Lane-level positioning and map matching are some of the biggest challenges for navigation systems. Additionally, in safety applications or in those with critical performance requirements (such as satellite-based electronic fee collection), integrity becomes a key word for the navigation community. In this scenario, it is clear that a navigation system that can operate at the lane level while providing integrity parameters that are capable of monitoring the quality of the solution can bring important benefits to these applications. This paper presents a pioneering novel solution to the problem of combined positioning and map matching with integrity provision at the lane level. The system under consideration hybridizes measurements from a Global Navigation Satellite System (GNSS) receiver, an odometer, and a gyroscope, along with the road information stored in enhanced digital maps, by means of a multiple-hypothesis particle-filter-based algorithm. A set of experiments in real environments in France and Germany shows the very good results obtained in terms of positioning, map matching, and integrity consistency, proving the feasibility of our proposal.**

***Index Terms*—Enhanced maps (Emaps), integrity provision, map matching, particle filter (PF), road vehicle navigation.**

I. Introduction

THE NUMBER of road vehicle services that demand positioning capabilities is continuously growing nowadays. Although vehicular telematics currently in the market provide services with positioning requirements that can be fulfilled by low-cost Global Navigation Satellite System (GNSS) receivers, the deployment of more complex road applications such as automated toll-collection systems or collision-avoidance support systems need a more reliable positioning subsystem [1]. A good example of these new requirements is the increasing interest in navigation at the lane level, with applications such as enhanced driver awareness, intelligent speed alert, and simple lane allocation [2].

In addition to an accurate value of positioning, the applicability of navigation systems to these applications depends on, first, the availability of an accurate common reference for the positioning [an enhanced map (Emap)] and, second, the level of reliability that the user can have on the provided pose estimation (its integrity). However, neither the current road maps nor the traditional integrity parameters seem to be well suited for these purposes.

On one hand, commercial maps that are currently available present a serious lack of accuracy, contents, and completeness for their applicability at the lane level. The accuracy level of standard maps today is around 5 (for metropolitan areas) to 20 m. The approximation of the road geometry by means of shape points introduces additional local errors. Finally, current maps severely simplify the road description. For instance, for a one-way road, a unique polyline is employed, regardless of the number of lanes of the carriageway, which is a simplification that is also assumed in some two-way roads with no physical separation between driving directions.

On the other hand, integrity parameters for road navigation have been imported from the aerial domain, despite the fact that many assumptions that are valid in the air are not verified in road scenarios [3]. The totally different conditions of satellite visibility or multipath effects demand a reconsideration of the integrity concept for roads. Furthermore, except for the case of car navigation on an absolutely unknown environment with no roads, the vehicle position must be referred to maps. Therefore, unlike in the aerial domain, new integrity indicators must cope with the map-matching process. Although there are attempts in the literature to provide integrity values for map-matching techniques, to the best of our knowledge, there is no reference to common integrity provision for both positioning and map matching.

This paper presents a pioneering approach to the problem of navigation and integrity provision at the lane level. A single data-fusion process based on a particle filter (PF) simultaneously performs both positioning and map matching by means of the measurements coming from a GNSS receiver,

Manuscript received March 10, 2009; revised August 3, 2009 and August 7, 2009. This work was supported in part by the Spanish Comisión Interministerial de Ciencia y Tecnología under Grant TIN2008-06441-C02-02 and in part by the Spanish Ministerio de Fomento under Grant FOM/2454/2007. This work was carried out in the frame of the European project Cooperative Vehicle Infrastructure Systems (CVIS) by researchers with the Geolocalization Group, Laboratoire Central de Ponts et Chaussees, partners of the Positioning and Mapping subproject POMA of CVIS, and the group of Intelligent Systems and Telematics/University of Murcia, awarded as an excellence researching group in frames of the Spanish Plan de Ciencia y Tecnología de la Regíon de Murcia under Grant 04552/GERM/06. The Associate Editor for this paper was F.-Y. Wang.

R. Toledo-Moreo is with the Department of Electronics, Computer Technology, and Projects, Technical University of Cartagena, 30202 Cartagena, Spain, and also with the Intelligent Systems Group, University of Murcia, 30003 Murcia, Spain (e-mail: rafael.toledo@upct.es).

D. Bétaille and F. Peyret are with the Laboratoire Central de Ponts et Chaussees, 44341 Bouguenais, France (e-mail: david.betaille@lcpc.fr; francois.peyret@lcpc.fr).

Color versions of one or more of the figures in this paper are available online at http://ieeexplore.ieee.org.

Digital Object Identifier 10.1109/TITS.2009.2031625

1524-9050/$26.00 © 2009 IEEE

Authorized licensed use limited to: Universidad de Cartagena. Downloaded on October 20, 2009 at 08:07 from IEEE Xplore. Restrictions apply.

This article has been accepted for inclusion in a future issue of this journal. Content is final as presented, with the exception of pagination.

a gyroscope, the odometry of the vehicle, and an Emap that describes the road geometry as linked lane segments. The system under consideration verifies the low-cost standards of cooperative systems, providing the following to the user:

1) lane allocation;
2) vehicle positioning on the lane, which is contrary to the most common approach in map matching of simply projecting the vehicle position on the center of the segment;
3) the relative lateral position of the vehicle on the carriageway, informing the user of how many lanes the carriageway has at its current cross section and on which one of these lanes the vehicle is;
4) a level of confidence on the position level that is based not only on GNSS measurements (as traditional integrity parameters do) but on the combination of all the sources of information employed in the positioning as well, including the Emap;
5) a level of reliability of the lane allocation, which is something that, to the authors' knowledge, has yet to be addressed in the literature.

Next, the state of the art in the field is discussed. The rest of this paper is organized as follows. Section III shows a description of our Emap paradigm. Next, Section IV presents the most significant aspects of the positioning cycle. Our approach for lane-level integrity is described in Section V. The test vehicles are presented in Section VI. Later, Section VII shows the results obtained in terms of positioning, map matching, and integrity provision. Finally, Section IX concludes this paper.

II. Related Work

The problem of road navigation based on GNSS positions (and possible combinations with some other sensors) is well treated in the literature. In [4], the authors survey at length in-car positioning and navigation technologies. A few other works of interest are [5]–[7].

In particular, it can be found that there is a rising interest in navigation at the lane level. The authors of [8] claim that many applications would benefit from this possibility and suggest a combination of a differential Global Positioning System (DGPS) receiver coupled with an Emap-matching algorithm. In [9], a solution based of the cooperation between vehicles that travel close to each other is presented. Wang *et al.* [10] present a system for lane keeping based on a Global Positioning System (GPS)/inertial navigation system and vision. Reference [11] shows how a combination of GPS and inertial sensors can be used to detect transitions between two lanes of the same carriageway. However, none of these works approach the issue of integrity at the lane level.

In previous publications by our team, the capability of performing lane-level navigation by means of an assisted GNSS plus an Emap has already been addressed [12]–[14]. Our investigations are now updated with improvements in the positioning method and the Emap and the inclusion of integrity provision to the system.

In navigation, integrity may be defined as the capability of the system to detect performance anomalies and warn the user whenever the system should not be used [15]. An approximation to provide integrity in GNSS-based navigation is given by the receiver-autonomous integrity-monitoring (RAIM) algorithm. This technique, which was initially created for aerial navigation, is based on the possibility, with an overdetermined solution, to evaluate its consistency, and therefore, it requires a minimum of five satellites to detect a satellite anomaly and six or more to be able to reject it [16]. In addition, the RAIM method makes the assumption that only one failure appears at the same time at the receiver. Unfortunately, these assumptions cannot be assumed in usual road traffic situations, particularly in cities [15].

Satellite-based augmentation systems such as the European Geostationary Navigation Overlay Service (EGNOS) or the Wide Area Augmentation System nowadays offer integrity calculation. By means of the information of the GNSS operational state, which is broadcast by geosynchronous orbit (GEO) satellites, it is possible to compute a meaningful parameter of navigation system integrity [17], [18]. However, due to the fact that the source of the integrity information comes from satellites, a lack of coverage implies the absence of updated integrity measurements. Moreover, the same assumption done in the RAIM technique of only one failure at the same time is also done in this approach, consequently with the same limitations at that respect [19].

All these problems encourage the search for some other different approaches to the problem of integrity in road navigation. Some authors based integrity on the confidence on the overall sensing system [15], [20], while some others test some new paradigms for GNSS error considerations [21]. Nevertheless, in these articles, the problem of posterior map matching is not addressed at all.

Although the problem of map matching is well covered in the literature of the field [22]–[29], only a few authors refer to the concept of integrity in map-matching algorithms [30], [31]. For this occasion, integrity is defined as the ability of mismatch detection and, in some cases, is tested *a posteriori* to compare different map-matching approaches. This concept of integrity, however, differs from the idea of integrity in navigation. Although positioning and map matching are linked in the largest majority of road-navigation applications, to the best of our knowledge, there is not yet a common solution for navigation and map-matching integrity.

III. Emap Description

Most geographical information systems (GISs) currently available represent roads with polylines (i.e., series of nodes and shape points, which are connected by segments). This representation corresponds only to some extent to the ground truth, being roads simplified to their centerlines. Additionally, what is modeled has limited accuracy from both the global and local points of view. Global and local errors, along with the missing contents, not only cause incorrect map matches but also prevent the development of applications that demand lane-level accuracy. Despite the fact that a few information items have been added to standard road maps to partially fulfill the requirements of advanced driver assistance systems (ADASs), such as the number of lanes (which can be stored as an attribute

Authorized licensed use limited to: Universidad de Cartagena. Downloaded on October 20, 2009 at 08:07 from IEEE Xplore. Restrictions apply.

This article has been accepted for inclusion in a future issue of this journal. Content is final as presented, with the exception of pagination.

of road segments) or the lanes' widths, further progress is still needed.

When roads are designed, a 2-D + 1 (separately for horizontal and vertical dimensions) series of straight lines, circles, and clothoids in the horizontal direction, as well as straight lines and parabolas in the vertical direction, is used. Therefore, one may expect similar mathematical structures hidden in the mobile mapping trajectories. Following this paradigm, [12] suggests a Kalman-based extraction process, where generalized clothoid parameters are identified. Clothoids have the advantage that their generic form may degenerate into circles or lines by simply zeroing one (for circles) or two (for straight lines) modeling parameters. An algorithm created by the authors and first presented in [12] is capable of automatically finding the clothoids that best fit a series of vehicle positions. However, the following preparatory manual operations are necessary before this happens.

1) Because there are Emap stretches that have been driven twice or more, redundant trajectories must be removed.
2) Since the total number of lanes or the driving regulations change at cross sections, the start and stop points of clothoids are fixed there.

The programmed extended Kalman filter processes already-smoothed GPS and dead-reckoning (DR) vehicle trajectories. The maximum deviation between the extracted geometry and the vehicle location was bounded to 5 cm. When an existing clothoid cannot be expanded without violating the aimed accuracy given by this threshold, this clothoid stops, and a new one starts. That way, the Emap meets the requirements of intelligent transportation system applications for positioning and mapping at lane-level accuracy. Finally, let us remark that, in our approach, consecutive clothoids are geometrically continuous with regard to the coordinates but not with regard to the heading and curvature.

Once the clothoids are extracted, the topology is next computed. Every clothoid is analyzed to list its neighbors and define whether these are located at the front, left, or right. The concept of neighbor segments is defined as follows: Segment B is a neighbor of segment A if a road vehicle can make a transition from segment A to segment B. Note that the fact that B is a neighbor of A does not imply that A is a neighbor of B. More concretely, if B is a front neighbor of A, a transition from A to B appears when the vehicle longitudinally leaves segment A. On the contrary, left or right neighbors can be reached by means of lateral movements. Later, it will be shown how knowing these attributes will accelerate the process of map matching.

A set of geometrical rules has been designed to automatically interconnect the segments and to create the topological description of the road. Further details on this process can be found in [12].

Fig. 1 shows the Emap generated near the Berlin-Adlershof German Aerospace Center (DLR) test site, Berlin, Germany.

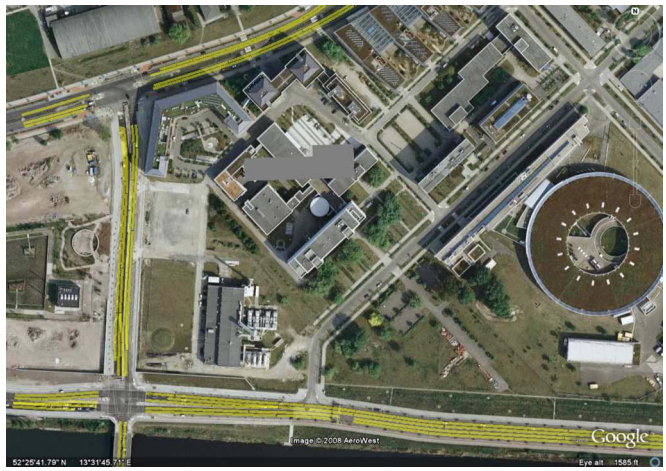

Fig. 1. Emap of the Berlin test site superimposed on the Google Maps image of the area.

IV. Positioning Cycle

This section presents a summarized description of the positioning cycle that fuses GNSS, DR, and Emap observations. For further details on its implementation, see [13]. In addition to the overview of the whole filter, the main improvements and new strategies are particularly stressed here.

The fusion process is based on a PF and is schematically represented in the flowchart in Fig. 2. As can be seen, apart from the usual stages of initialization, prediction, and normalization, we can notice that there are two steps of update, whether with Emap or with GNSS observations. The nature of these observations encourages us to employ a double-reference system. Thus, the state vector consists of a combination of Frenet and Cartesian coordinates, which represent the same vehicle position any time in two different reference frames, and will be employed in the updating process, depending on the nature of the observations. In the following sections, the relation between both reference systems and each filter stage is briefly described.

A. Frenet and Cartesian Frames

The state vector of our filter is a composition of a Cartesian and a Frenet substate, i.e., $\mathbf{X} = [\mathbf{X}^C, \mathbf{X}^F]$, where $\mathbf{X}^C$ stands for the Cartesian part and $\mathbf{X}^F$ for the Frenet one (in the following, these superscripts will be used to distinguish both subsystems). $\mathbf{X}^C$ is defined by $[x, y, \psi]$, representing east, north, and the heading angle, respectively, at the point of the GNSS antenna, while $\mathbf{X}^F$ includes $[l^m, d^m, m]$, which represent the values of the abscissa and ordinate referred to the lane segment m. The state variables of the proposed filter are represented in Fig. 3.

The inclusion of Cartesian and Frenet definitions for the same point introduces a partial redundancy in the state vector, which implies some particularities in the implementation of the PF. On the other hand, it brings some benefits to its implementation.

1) Frenet variables are more adequate for evaluating the transitions between lane segments of the road and applying Emap observations.
2) The east and north values for positioning are necessary in a number of location-based services. In addition to that, the inclusion of a Cartesian substate also allows uninterrupted navigation when the Emap reference is not present.

Authorized licensed use limited to: Universidad de Cartagena. Downloaded on October 20, 2009 at 08:07 from IEEE Xplore. Restrictions apply.

This article has been accepted for inclusion in a future issue of this journal. Content is final as presented, with the exception of pagination.

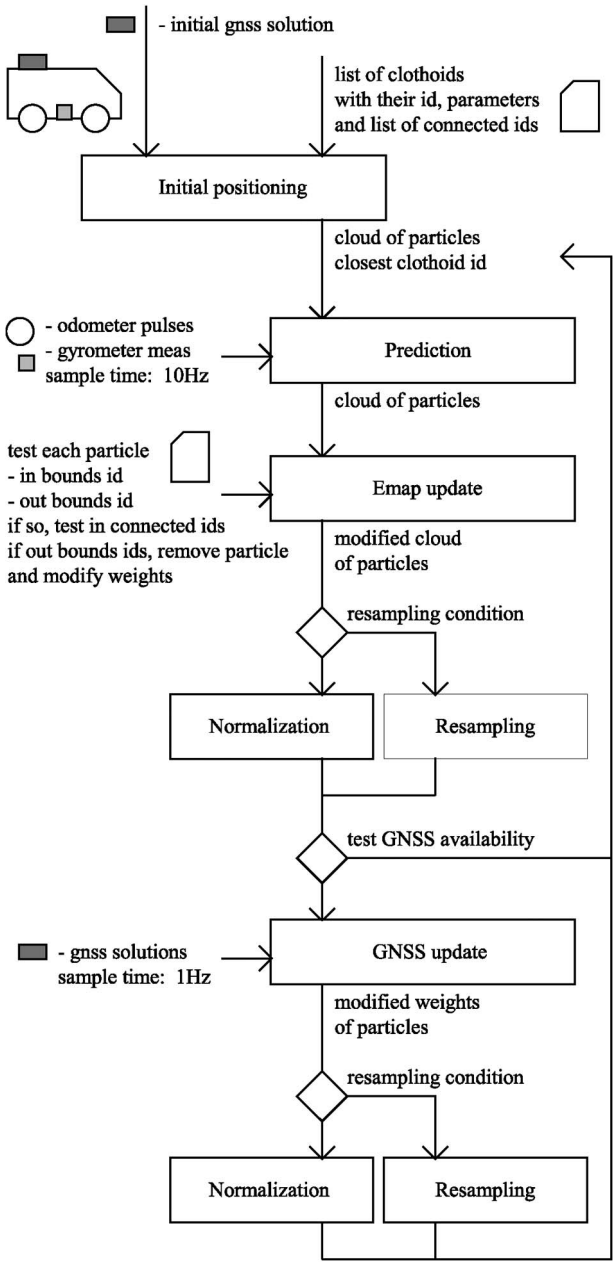

Fig. 2. Flowchart of the GNSS/DR/Emap fusion process.

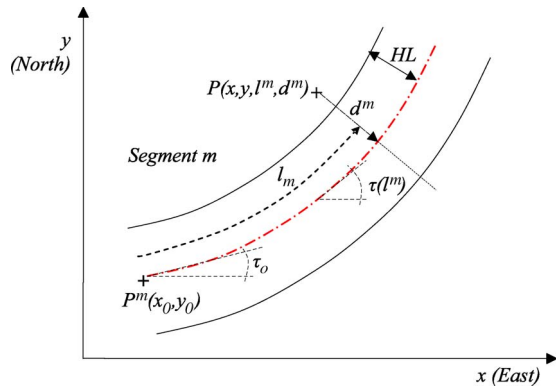

Fig. 3. Cartesian x- and y-coordinates and Frenet l^m- and d^m-coordinates for a point P and the position of a vehicle driving segment m with a given half of a lane width HL. Initial angle of the segment τ_0 and angle at any Frenet abscissa $\tau(l_m)$.

The state vector that represents a particle i at instant k according to the variables presented in Fig. 3 is given by

$$X_k^i = \left[x_k^i, y_k^i, \psi_k^i, l_k^{m,i}, d_k^{m,i}, m_k^i\right]. \tag{1}$$

Both Frenet and Cartesian representations of the same point are related by the expression

$$\begin{aligned} x &= x_0^m + \int_0^{l^m} \cos\left(\tau^m(l^m)\right) dl - d^m \sin\left(\tau^m(l^m)\right) \\ y &= y_0^m + \int_0^{l^m} \sin\left(\tau^m(l^m)\right) dl + d^m \cos\left(\tau^m(l^m)\right) \end{aligned} \tag{2}$$

where x_0^m and y_0^m are the east and north coordinates of the initial point of the road segment, and $\tau^m(l^m)$ is the azimuth angle of the segment at abscissa l^m, which is given by

$$\tau^m(l^m) = \tau_0^m + \kappa_0^m \cdot l^m + \frac{c^m \cdot (l^m)^2}{2} \tag{3}$$

with τ_0^m, κ_0^m, and c^m being the shape parameters for segment m and representing, respectively, the initial heading, the initial curvature, and the linear curvature rate of the clothoid (see Fig. 3).

B. Initialization

The filter begins with the initialization of the particles X_0^m. To realize this, first, the Cartesian substate variables x and y are randomly generated following a Gaussian distribution with the first accepted GNSS point as mean value and a standard deviation value according to the GNSS *a posteriori* solution statistics. Since it is assumed that no information about the initial heading is available, the values of ψ^i are uniformly spread through the whole range of 2π rad.

For the initialization of the variables of the Frenet substate $X_0^{F,i}$, we must first find out the lane segment in which each particle of the corresponding Cartesian substate $X_0^{C,i}$ is placed. With no *a priori* information on the vehicle position or orientation, we can simply assign the particle to its closest road segment $m(i)$. The Frenet variables referred to it, i.e., $[l^{m,i}, d^{m,i}]$, can directly be obtained since $d^{m,i}$ is the minimum distance between $[x^i, y^i]$ and segment $m(i)$, and $l^{m,i}$ is its corresponding abscissa in the Frenet system (see Fig. 3). As can be noticed, $d^{m,i}$ is actually the value of the shortest distance found when searching the corresponding segment $m(i)$.

C. Filter Prediction

The prediction of the Cartesian substate for each particle will be calculated in the following:

$$\begin{aligned} x_{(k|k-1)}^i &= x_{k-1}^i + \Delta_x^i \\ y_{(k|k-1)}^i &= y_{k-1}^i + \Delta_y^i \\ \psi_{(k|k-1)}^i &= \psi_{k-1}^i + \omega^i \end{aligned} \tag{4}$$

Authorized licensed use limited to: Universidad de Cartagena. Downloaded on October 20, 2009 at 08:07 from IEEE Xplore. Restrictions apply.

This article has been accepted for inclusion in a future issue of this journal. Content is final as presented, with the exception of pagination.

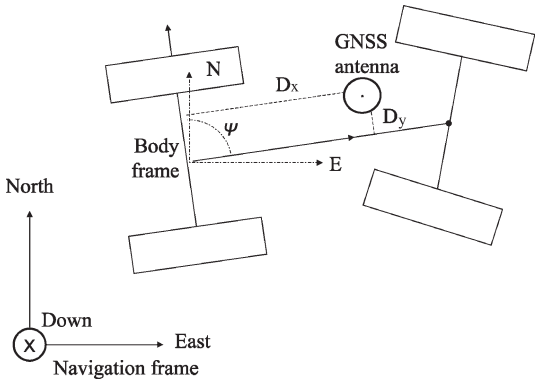

Fig. 4. Scheme of the vehicle model and body and navigation reference frames.

where

$$\Delta_x^i = ds^i \mathrm{sinc}(\omega^i/2)\cos(\psi^i + \omega^i/2) - \omega^i\left(Dx\sin(\psi^i) + Dy\cos(\psi^i)\right) + \delta_x^i \quad (5)$$

$$\Delta_y^i = ds^i \mathrm{sinc}(\omega^i/2)\sin(\psi^i + \omega^i/2) + \omega^i\left(Dx\cos(\psi^i) + Dy\sin(\psi^i)\right) + \delta_y^i \quad (6)$$

and the other variables are described as follows.

1) ω^i is an input of the filter and represents the vector of angular velocity values for every particle, following $\omega^i \sim N(\omega_{\mathrm{gyr}}, \sigma^2_{\mathrm{gyr}})$, where ω_{gyr} is the gyro measurement of the heading rate, and σ^2_{gyr} is its variance, which can be characterized using the angular random walk provided by its manufacturer.
2) ds^i is an input of the filter and represents the vector of traveled distances for every particle, which can be calculated by adding to the measurement of the traveled distance by the odometer ds_{odo} a uniform distribution of noise around $[-step_{\mathrm{odo}}, step_{\mathrm{odo}}]$, where $step_{\mathrm{odo}}$ is the odometry step equal to 0.2615 m in our case.
3) Dx and Dy are the Cartesian distances in the body frame of the vehicle between the position of the antenna and the middle point of the rear-wheel axle, where the vehicle pose model is assumed to be applicable (see Fig. 4).
4) δ_x^i and δ_y^i stand for the errors in the prediction of $x^i_{(k|k-1)}$ and $y^i_{(k|k-1)}$ in the navigation frame, which are modeled as random-walk processes in such a way that, after 1 s, the error due to the model inaccuracy is assumed to be 0.2 m, which was found to be a suitable tuning for our algorithm.

The terms Δ_x^i and Δ_y^i represent the variation with respect to the previous step of the x^i and y^i state variables for a particle. Since both Frenet and Cartesian representations must be consistent, the prediction of the Frenet variables depends on these terms.

In [13], the prediction of Frenet variables is carried out following

$$l^{m,i}_{(k|k-1)} = l^{m,i}_{k-1} + \cos\left(\tau^{m,i}_{(k|k-1)}\right)\Delta_x^i + \sin\left(\tau^{m,i}_{(k|k-1)}\right)\Delta_y^i$$
$$d^{m,i}_{(k|k-1)} = d^{m,i}_{k-1} + \sin\left(\tau^{m,i}_{(k|k-1)}\right)\Delta_x^i - \cos\left(\tau^{m,i}_{(k|k-1)}\right)\Delta_y^i. \quad (7)$$

However, it was found that the assumption of straight movements between samples made in (7) was too strict in the case of a highly curved road segment, leading to an accumulative error in the Frenet frame that, in some cases, reached some decimeters. Although these errors are zeroed during segment transitions and resamples, a better solution is now proposed. The proposed new method is based on updating the angular information between consecutive positions a number of times NF, which is capable of guaranteeing a much more precise approximation. To do it, the estimation of $l^{m,i}_{(k|k-1)}$ and $d^{m,i}_{(k|k-1)}$ is iteratively carried out a sufficient number of times, with $NF > 1$, applying Δ_x^i/NF and Δ_y^i/NF spatial increments until $\tau^{m,i}_{(k|k-1)} \approx \tau^{m,i}_{(k|k)}$, where the index j stands for the multiple increments

$$l^{m,i,j}_{(k|k-1)} = l^{m,i,j-1}_{k-1} + \cos\left(\tau^{m,i,j-1}_{(k|k-1)}\right)\Delta_x^i/NF + \sin\left(\tau^{m,i,j-1}_{(k|k-1)}\right)\Delta_y^i/NF$$
$$d^{m,i,j}_{(k|k-1)} = d^{m,i,j-1}_{k-1} + \sin\left(\tau^{m,i,j-1}_{(k|k-1)}\right)\Delta_x^i/NF - \cos\left(\tau^{m,i,j-1}_{(k|k-1)}\right)\Delta_y^i/NF. \quad (8)$$

A number of iterations $NF = 50$ showed significant improvements without costing much additional computational charge. Indeed, the error in the prediction of the Frenet substate was diminished by around ten times (to only a few centimeters in the worst cases), while computations still meet real-time requirements.

D. Emap Update

The prediction cycle presented in Section IV-C is applied at every input sample. However, these predictions will only be considered as valid when the pose predicted for a particle i is still within the bounds of the segment associated with this particle at the instant that the prediction is made ($m_{(k|k-1)} = m_{(k-1)}$). Therefore, after every prediction phase, the condition given by the following equation must be verified by using the Emap observations:

$$\left(0 < l^{m,i}_{(k|k-1)} < L^m\right) \quad \text{and} \quad \left(-HL < d^{m,i}_{(k|k-1)} < HL\right) \quad (9)$$

where L^m is the length of the segment (stored in the Emap), and HL is the value for half of a lane width, which is assumed to be constant in our tests and equal to 2.25 m. The assumption of constant lane width may raise some problems in the Emap update phase: A particle may be considered out of a lane when it is not and *vice versa*. Nevertheless, it was found during the experiments carried out that this assumption is not very severe and that the consequences are not significant.

In case (9) is satisfied, the prediction performed in (8) is accepted, and $m_k = m_{(k-1)}$. If any prediction of the Frenet variables does not verify (9), the results of (8) must be disregarded, and a different process must be followed. In this last case, two possibilities arise.

1) The vehicle moved from the previous segment to a different one, i.e., $m_k \neq m_{(k-1)}$, with m_k being the new segment linked to the m_{k-1} in the Emap.

Authorized licensed use limited to: Universidad de Cartagena. Downloaded on October 20, 2009 at 08:07 from IEEE Xplore. Restrictions apply.

This article has been accepted for inclusion in a future issue of this journal. Content is final as presented, with the exception of pagination.

2) The vehicle is not within the bounds of any road segment, and this particle must be eliminated, making its weight $w_k^i = 0$.

A new improvement is being applied in this process. As has been mentioned previously, new Emaps store an indicator of the nature of the connectivity between a segment and its neighbors. The description of a neighbor as front, left, or right brings geometrical information of interest that may now be applied. On one hand, the algorithm is more robust, since particles can only move to segments that are topologically feasible, eliminating unfeasible allocation hypotheses due to the spread of the cloud of particles. On the other hand, in this new approach, when a particle leaves a segment, the search for its new segment is guided by the Frenet variables, decreasing the number of lanes of the search by typically around three times. Therefore, if (9) is not verified because $d^{m,i}_{(k|k-1)} > HL$, only right neighbors will be checked, and so forth, for the rest of the cases. This significantly reduces the computational time of this process.

E. GNSS Update

When valid GNSS measurements are available, a GNSS update will be carried out. This update is the common step performed in PFs for positioning with bootstrap configuration, and it has been further explained in [13].

F. Normalization and Resample

After every update phase, the weights of the particles are subject to be modified, and the usual normalization and resample test phases of a PF must be launched.

V. Integrity Definition

As has been previously discussed in this paper, in spite of its clear benefits, the concept of integrity in navigation has never been addressed in the literature with regard to a map-matched position of a road vehicle at the lane level. This section summarizes our proposal for this challenging aim. Nevertheless, due to its great interest, the study of this concept and its implementation is continuously ongoing.

The integrity concept applied to the problem of combined fusion and map matching by using GNSS, DR, and Emap observations should focus on two different aspects:

1) correct lane assignment;
2) the confidence on the position of the vehicle on the assigned lane.

Naturally, the latter aspect absolutely depends on the first one: It is not possible to establish a level of confidence on the position on a segment if it is not clear to which segment the vehicle should be referred. Therefore, the second aspect can be achieved conditionally to the first.

Consequently, a definition of integrity for the problem under consideration should do the following:

1) Embrace the capability of the system to correctly identify the lane segment on which the vehicle is at every epoch, detecting the possible mismatches in the segment assignment.

TABLE I
Examples of K_{LPPL} Values Associated to P_{md} Objective Values

P_{md}	0.1	0.01	0.001	10^{-9}
K_{LPPL}	2.146	3.034	3.717	6.18

2) Accurately estimate the vehicle position on that lane with relevant confidence indication.

The distinction between a confidence level on the map-matching process and a protection level (in meters) of the position itself may be found to be beneficial in a number of applications. Let us put the example of a vehicle circulating through a tunnel with a single lane in a single direction. In this simple example, it appears to be clear that our confidence on the segment assignment must be very high, since it is not feasible for the vehicle to leave the lane through the tunnel. On the other hand, due to the increasing uncertainties in the measurements and vehicle models without the application of GNSS updates, the confidence on the vehicle position should be low. These two aspects must therefore be reflected in the confidence on the final navigation solution (which includes, of course, the effect of the map observations).

In our proposal, two variables represent the integrity level of the map-matched position of the vehicle, which are explained next.

A. Lane Occupancy Probability (μLO)

The probability that the vehicle occupies lane segment r at instant k, i.e., $\mu_k^{m=r}$, can be calculated as the addition of the normalized weights of the particles that are associated with segment r, following the next expression:

$$\mu_k^{m=r} = \sum_{i=1}^{N} w_k^{i|m=r}. \tag{10}$$

Since both positioning and map matching are simultaneously performed by our filter, this parameter is representative of the level of confidence of both navigation operations.

B. Lane Positioning Protection Level (LPPL)

This second parameter will be analogous to the protection-level parameters coming from the aerial navigation described in [32] and will follow the equation

$$\mathrm{LPPL} = K_{\mathrm{LPPL}} \times \sigma_{\mathrm{pos}}$$

where K_{LPPL} can be calculated with the Rayleigh inverse cumulative distribution function (we assume two dimensions and $\sigma = 1$) and will indicate how cautious we are when we provide a protection level

$$K_{\mathrm{LPPL}} = \mathrm{Rayleigh}(\sigma = 1)^{-1}(1 - P_{\mathrm{md}})$$

with P_{md} being the probability of missed detection (MD) selected. This value will be fixed according to the needs of the intended application. Table I gives some examples. For our experiments, we fix it at 3.034.

The value of σ_{pos} can be estimated as the maximum eigenvalue of the covariance matrix for the position in the x- and

Authorized licensed use limited to: Universidad de Cartagena. Downloaded on October 20, 2009 at 08:07 from IEEE Xplore. Restrictions apply.

This article has been accepted for inclusion in a future issue of this journal. Content is final as presented, with the exception of pagination.

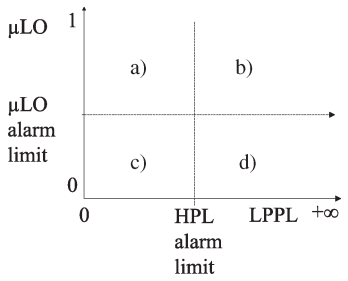

Fig. 5. Cases of integrity alarm.

y-coordinates. Note that, since we take the maximum of the eigenvalues, we obviously obtain a circle, and using the state variables of the Frenet substate would lead to the same result.

Once again, σ_{pos} already embraces the result of positioning and map matching at once.

C. Double Integrity Indicator

It may look that the integrity indicators just presented may be contradictory in some cases, such as the example of the vehicle in a tunnel previously exposed. Indeed, as the vehicle drives through the tunnel, the value of the LPPL grows with time due to the lack of GNSS updates, and μLO remains one. However, both parameters may be used to offer a more useful picture of the integrity state of the vehicle. It is actually true that we may have a very low confidence on the position, while we are still very sure that the vehicle is on one lane. Furthermore, it is even possible that one parameter can benefit from the other. For instance, a very high value of confidence on the segment assignment would constrain the rise of the LPPL value since the particles with predicted positions out of the bounds of the lane segment will be eliminated from the filter solution (their weights will be zeroed). The convenience of both indicators is clear.

Fig. 5 shows all possible combinations of these integrity indicators, as referred to their corresponding alarm limits for an intended application. Let us analyze each of them and their implications.

a) This is the usual case of being very confident about the position and the map matching.
b) This case can be represented by the aforementioned example of the tunnel or, more generally, with a vehicle travelling through a single road in an area of bad satellite view.
c) This is the case of a vehicle with good GNSS visibility that circulates in between two lanes (for instance, as a consequence of an overtaking maneuver).
d) This is the typical case of losing GNSS coverage for a long period when driving in a carriageway with multiple lanes. With time, the LPPL grows enough for the particles to cover all the lanes of the carriageway, and the μLO decreases as the particles move to adjacent lanes.

The decision of whether firing an alarm associated with an intended application depends on the nature of the application and on the selected strategy. For example, if the intent is to diminish the number of false alarms (FAs) in an ADAS application where errors due to a *GO* decision are less tolerated than errors due to *NO GO*, the only case in which the alarm should be fired is case a). On the contrary, an application of the onboard speed limit indicator could be launched in cases a) and b).

TABLE II
EXPERIMENTAL SCENARIOS

Scenario	Circuit	Duration	Sensors	GNSS mask
S1	Nantes semiurban	617 s	EGNOS+ FOG+Odo.	Sparse gaps of (3–4) s
S1M	Nantes semiurban	617 s	EGNOS+ FOG+Odo.	Sparse gaps + 4 × 32 s
S2	Nantes semiurban	104 s	EGNOS+ FOG+Odo.	Null
S2M	Nantes semiurban	104 s	EGNOS+ FOG+Odo.	22 s
S3	Berlin semiurban	224 s	EGNOS+ MEMS+CAN	Sparse gaps of (1–2) s
S3M	Berlin semiurban	224 s	EGNOS+ MEMS+CAN	Sparse gaps + 3 × 12 s

VI. EXPERIMENTAL SETUP

Different experiments were done in Nantes and Berlin with two prototypes. The test vehicles were equipped as follows.

1) In Nantes, a van was equipped with an external odometer on the left rear wheel, 1 pulse per 0.2 m, a KVH e-core 2000 series gyro, and a 10-Hz digital output model. Two GPS receivers were set up on board: one (Trimble Ag132) using EGNOS satellite broadcast and the other (Thales Scorpio) logging dual-phase measurements for further kinematic postprocessing with a local base station. A reference trajectory was obtained that way.
2) In Berlin, a car was equipped with the control area network (CAN) vehicle speed, a microelectromechanical system (MEMS) analog device gyro component, and, again, a pair of GPS receivers—one (μBlox) using EGNOS and the other (Trimble 5700) using SAPOS network dual-frequency kinematic data.

VII. EXPERIMENTAL RESULTS

Table II summarizes the main features of the different tests employed in our experimentation. In addition to the description provided in the table, the notation used to indicate whether the Emap was employed in these scenarios goes like this: SXE indicates the use of Emap in scenario SX, while SX indicates its absence. Similarly, M stands for additional GNSS simulated masks. The navigation results of all the circuits presented in Table II are shown in the next section with and without Emap observations. On the contrary, map-matching and integrity results are intrinsically linked to the use of the Emap, and hence, they can only be analyzed for the scenarios when the Emap was employed.

As can be noticed, the vehicle instrumentation in both test sites was different. This impedes a direct comparison between the results achieved with both sets of equipment. However, it shows the capability of the algorithm under proposition to work with several sensor configurations, which is of the most interest in the analysis of its results. The errors obtained by low-cost sensors, such as MEMS gyroscopes, are typically larger than those obtained with fiber-optic gyro (FOG) devices, and

Authorized licensed use limited to: Universidad de Cartagena. Downloaded on October 20, 2009 at 08:07 from IEEE Xplore. Restrictions apply.

This article has been accepted for inclusion in a future issue of this journal. Content is final as presented, with the exception of pagination.

TABLE III
HPEs IN M IN DIFFERENT TEST SCENARIOS

Test	Mean	Std	Max.
S1	0.309	0.296	2.468
S1M	0.580	0.795	4.049
S1E	0.289	0.287	2.277
S1ME	0.389	0.405	2.317
S2	0.660	0.698	2.002
S2M	0.800	0.619	2.007
S2E	0.691	0.709	2.088
S2ME	0.876	0.658	2.028
S3	0.261	0.274	1.915
S3M	4.849	6.635	20.048
S3E	0.296	0.324	2.289
S3ME	0.279	0.426	2.944

therefore, the overall accuracy of the MEMS approach appears lower. However, for both devices, the integrity of the system should not be compromised. This aspect will be discussed in Section VII-C.

A. Navigation Results

In this section, we focus on the performance of the navigation system itself. Our main purpose is to validate the consistency of the results of whether the visibility of the GPS satellites is good and to verify the potential benefits of the use of an Emap to assist in the navigation process.

The estimates of the horizontal errors presented next are obtained by comparing the (east and north) output of the filter with the assumed truth, which is given by the DGPS carrier phase receiver introduced in Section VI.

Table III shows the results of the horizontal positioning errors (HPEs) for the different scenarios introduced in Table II with and without Emap updates.

As can be seen, the differences between using and not using the Emap in cases of good GPS coverage are not high with respect to navigation. However, when GPS masks longer than 1 or 2 s appear, the results obtained in those cases in which the Emap was applied are more consistent and much more suitable for a navigation system that aims at the lane level. Indeed, HPE values over 3.5 m are clearly unsuitable for distinguishing between adjacent lanes. This can be found to repeatedly appear along all the different tests of our experiments, becoming particularly remarkable in the experiments with low-cost sensors, such as the comparison between S3M and S3ME.

We can analyze in more detail these errors by observing Fig. 7, which shows the value of the HPE in time for (top) scenarios S1 and S1E and (bottom) scenarios S1M and S1ME. In scenario S1, with good GNSS coverage, the differences between using and not using the Emap observations are not so remarkable. Nevertheless, as shown in Table III and can graphically be noticed in the image, particularly in the zoomed view of this image for the stretch during instants 10 and 70 s, the use of the Emap is still beneficial. However, the improvements are even clearer in the images of the experiments carried out in scenario S1M. When the Emap is applied, the estimate of the vehicle position stays within the limits of the road lanes.

Apart from avoiding drifts out of the feasible positions of the vehicle, the Emap updates can be found to be useful in preventing GNSS outliers that can be difficult to detect by most common tests such as the Nyquist test applied in our algorithm based on the Mahalanobis distance [33]. Fig. 6 shows an example of this situation in the test in Berlin. The level of confidence is schematically represented by means of green ellipses of the 2σ envelope of the horizontal error estimates, assuming a Gaussian distribution. Rejected GNSS positions are represented by $\diamondsuit$ symbols. The confidence on the vehicle model decreases with time until the next valid GNSS update. However, the error estimates of the vehicle positioning are still affected by the Emap updates and bounded by the road geometry and topology. In this example, segments 8 and 21 are not linked in the Emap. As can be seen, its growth is dependent on the feasibility of a maneuver in terms of lane restrictions, which causes the correct systematic invalidation of GNSS updates there.

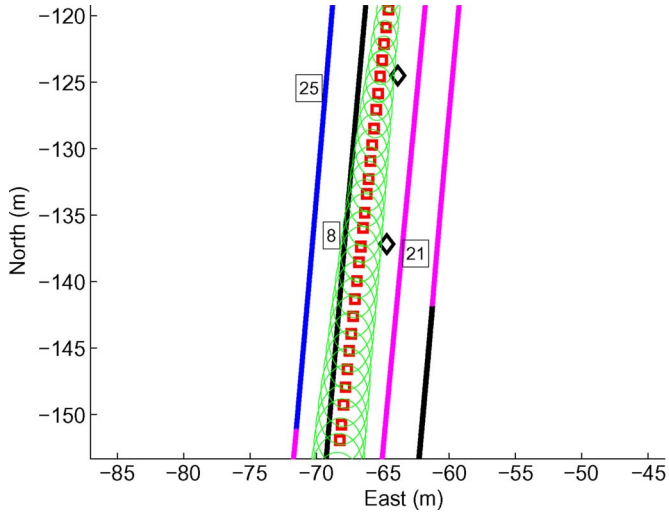

Fig. 6. Example of GNSS outlier rejection by means of the Emap. The Emap updates bound the error estimate (represented by green ellipses) within the feasible maneuvers regarding road topology and geometry. The consequence is that the ellipses of confidence do not grow where the vehicle cannot travel. Since segments 8 and 21 are not linked in the Emap, the GNSS outliers ($\diamondsuit$) are correctly eliminated from the filter solution.

Despite its benefits regarding GNSS outlier detection, the rejection of aberrant data, typically as a consequence of multipath effects, cannot exclusively be based on the topological description of the road if we aim for an integer system. A combination of a Nyquist test and the Emap observations avoids some of these problems, but in the authors' opinion, there is a clear need for an efficient algorithm capable of detecting GNSS outliers and whether to remove the aberrant data from the position estimation or to simply estimate the impact of these aberrations on the GNSS position and accordingly warn the system. The peak values observed in Fig. 7 are, as a matter of fact, a consequence of nondetected spurious GPS positions that still lie on an area considered to be feasible by the Emap observations.

Due to the importance of this topic, some investigations are being carried out by our research group [19]. Nevertheless, we consider that they are out of the scope of this paper.

B. Map-Matching Results

By means of DGPS carrier phase solutions of high accuracy, the vehicle position is manually assigned to the most likely lane segment at every epoch. In those cases where the assignment

Authorized licensed use limited to: Universidad de Cartagena. Downloaded on October 20, 2009 at 08:07 from IEEE Xplore. Restrictions apply.

This article has been accepted for inclusion in a future issue of this journal. Content is final as presented, with the exception of pagination.

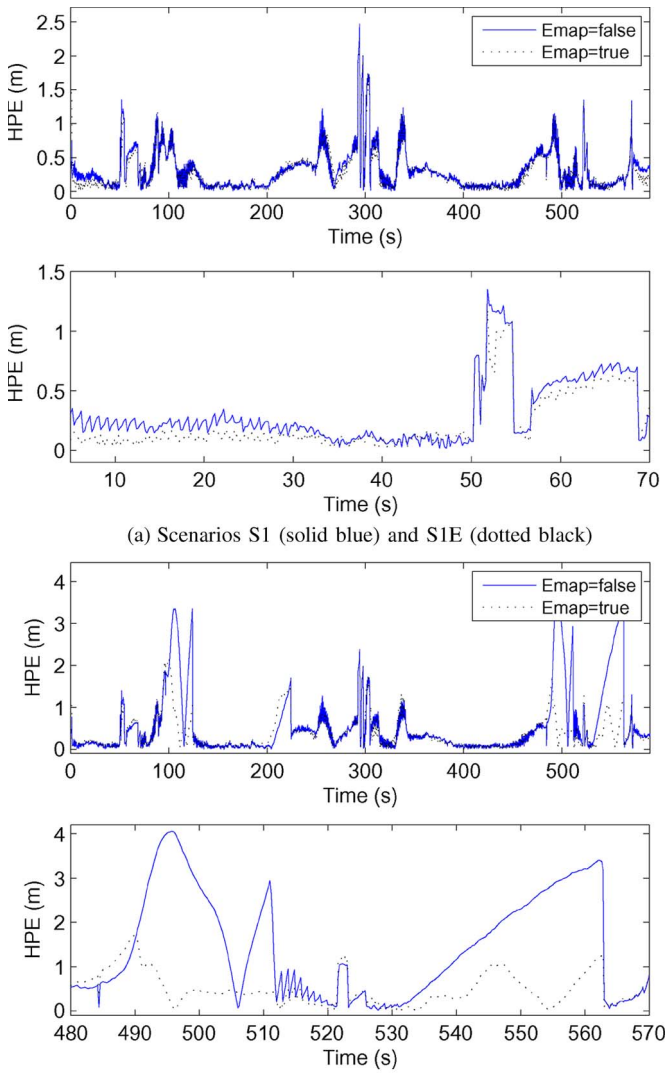

(a) Scenarios S1 (solid blue) and S1E (dotted black)

(b) Scenarios S1M (solid blue) and S1ME (dotted black)

Fig. 7. Estimates of the HPE values of the S1 and S1M tests in Nantes, France. (a) Top: Complete trajectory during the S1 test with some sparse gaps in the GNSS signal and GNSS outliers. Bottom: Zoom-in of the initial stretch. Scenarios S1 (solid blue) and S1E (dotted black). (b) Top: Complete trajectory of test S1M. Bottom: Zoom-in during one of the GNSS outages of 32 s plus some sparse gaps in the GNSS signal and GNSS outliers. In both scenarios, peaks around instant 300 s correspond to aberrant GNSS positions due to multipath effects. Scenarios S1M (solid blue) and S1ME (dotted black).

is not clear (for instance, when two wheels of the vehicle are on a lane and the other two on another), we decided against including them in the subset of mismatches. The results regarding map matching and correct lane assignment obtained from the different test scenarios in Table II are presented in Table IV and discussed in this section. As has been commented, for obvious reasons, only the tests with Emaps can be considered for map matching.

Let us remind the reader that these results also correspond to lane assignment and not only to road assignment. In all the scenarios tested in our experiments, the percentage of correct matches to the road is 100%. In the worst case among all tests, where, 16% of the time, the GNSS was masked and some sparse GNSS outliers appeared, 98% of the lane assignments made by our algorithm were found to be good. In the best case, 100% of the lane assignments were actually correct.

TABLE IV
MAP-MATCHING RESULTS

Test Scenario	Mismatch percentage	Mismatch time	GNSS blockage duration
S1E	0.6 %	3.5 s	13 s
S1ME	1.8 %	10.9 s	141 s
S2E	0.0 %	0.0 s	0 s
S2ME	1.8 %	1.8 s	22 s
S3E	1.3 %	2.9 s	9 s
S3ME	1.9 %	4.43 s	45 s

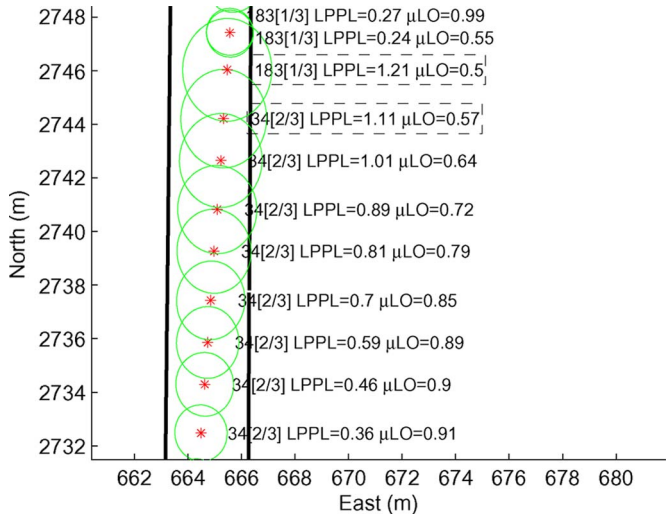

Fig. 8. Example of lane change. Solid black lines represent the median line for each lane. The information provided to the user during the maneuver consists of the segment ID, the relative lateral position of the segment on the carriageway and the number of lanes on the carriageway (in between squared brackets), and the values of LPPL and μLO. The red stars stand for the positioning outputs of the filter, while the green ellipses represent the 2σ envelope for the estimated horizontal positioning errors, assuming a Gaussian distribution.

Additionally, we must consider that our system provides integrity indicators of the quality of the positioning and map matching, which means that, for some of the mismatches, the user is informed that there is a high risk of incorrect segment assignment. This information can be found to be very useful in deciding whether or not to launch an ADAS application at the lane level.

C. Integrity Analysis

As introduced in Section V, in our approach, two parameters are in charge of notifying when the system should not be used by an intended application. These two parameters are now illustrated in the image in Fig. 8, where the values of the integrity parameters μLO and LPPL are shown during a lane-change maneuver from segment 34 (left lane) to segment 183 (right lane). As can be noticed, without a GNSS update, the value of the LPPL increases, due to the decreasing confidence of the filter on its output position. The larger dispersion of the particles and their weights also influences the value of the probability of lane occupancy. As long as particles lie outside the limits of segment 34, the confidence on the lane assignment must decrease, and so, it is noted by the parameter μLO. The moment of the transition between both segments has been enhanced by an edge box in the image. Once the switch is performed, the probability of segment 183 increases (from 0.5 to 0.55). When

Authorized licensed use limited to: Universidad de Cartagena. Downloaded on October 20, 2009 at 08:07 from IEEE Xplore. Restrictions apply.

This article has been accepted for inclusion in a future issue of this journal. Content is final as presented, with the exception of pagination.

a new GNSS position arrives, the particles and their weights are redistributed, affecting the value of LPPL and μLO. Since the confidence on the position is much higher, μLO becomes near one (0.99), and LPPL reaches the values corresponding to a GPS/EGNOS update. The low values of LPPL and μLO indicate a lane change carried out under good conditions for the positioning. This way, although the values of μLO are low at some instants, due to the LPPL indicator, the overall confidence on the navigation and map matching can be found to be high.

Of special interest is how the use of both indicators results in being beneficial for applications that demand the detection of lane changes. While the decision of whether a vehicle has changed lanes can be based only on μLO (when the value of μLO for the lateral neighbor segment is higher, the lane change has been completed), LPPL gives a measure of the system confidence on this information. For LPPL values over a certain threshold, caution is recommended since the navigation conditions may be not good enough for deciding at the lane level of detail. An example of this can be found in Fig. 8. In the upper part of the image, it can be seen how when the vehicle changes lanes (initially, it is allocated in segment 183), the value of LPPL is 1.21. An application demanding very high certainty on the lane change may find this value to be too high. However, just in the next step, the value of LPPL falls to 0.24, which is around five times more accurate, making it possible to launch the intended application.

1) Study of Mismatches: In Section VII-B, the results of lane assignments along all the test scenarios were shown. We will now discuss the status of the integrity indicators during these tests. There are typically two main reasons for a lane mismatch.

1) Errors due to undetected GNSS outliers. In case of undetected GNSS outliers (undetected by means of GNSS measurement integrity tests), the values of the LPPL indicator will not be affected, showing high confidence on the positioning. In this scenario, two things may occur. First, the outlier leads to an error in the position that is found to be feasible by the Emap observations, and therefore, the error is not detected by the integrity indicators. Against this, more efficient GNSS fault detection and exclusion algorithms must be developed, which is out of the scope of this paper. Second, the Emap observations may correct the outlier if the road geometry and topology prevents changing from one segment to another (as in the example in Fig. 6).
2) Errors due to drifts in the vehicle position as a consequence of a long GNSS blockage or a series of GNSS positions being rejected in the GNSS integrity test. In this case, depending on the road topology, both integrity parameters must reflect the situation, providing useful information about the actual reliability of the system.

Examples of these two cases can be found in the scenarios previously analyzed. The first reason, i.e., GNSS outliers, is the case of all the mismatches during scenario S1E, in which the mismatches correspond to GPS outliers that are assumed to be good in a stretch where two lanes are merging into one. Paying attention to the images in Fig. 9, we can obtain

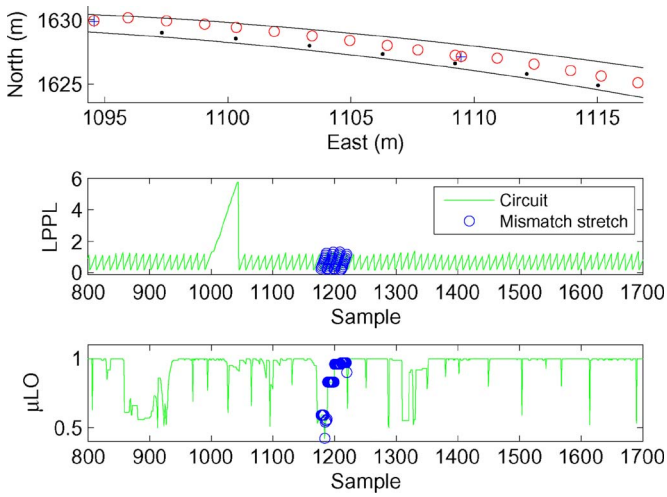

Fig. 9. (Top) Stretch of estimated vehicle trajectory where mismatch occurs in S1E. Road lanes (solid black), ground truth (black ·), and filter positions (red o), GPS/EGNOS positions (blue +). (Middle) LPPL values along a stretch of the circuit (solid green) and during the period of mismatch (blue o). (Bottom) μLO values along a stretch of the circuit (solid green) and during the period of mismatch (blue o).

some conclusions. The distance between the centerlines of both lanes is short (around 1.5 m) at this stretch of the road. GNSS positions are biased to the direction of the right lane, as compared with the ground truth. Since GNSS positions are assumed to be good, LPPL values supply no information about the mismatch. μLO values show a noticeable diminution when the vehicle "changes lanes" according to the estimates of the filter. However, setting the alarms in such a way that the user would be warned in this situation would also fire them every time the vehicle realizes a lane change.

With regard to the second reason, a good example of lane-assignment error due to a drift in the vehicle position estimate appears in scenario S3ME. In the images in Fig. 10, we can see, during a long GNSS gap, how the estimate of the vehicle position drifts, progressively invading the contiguous lane. Both parameters reflect this situation with high values of LPPL (over 5 m) and low values of μLO (close to 0.5) during the period of mismatch. It can be accepted that the user is warned of the unreliability of the navigation and map-matching solution.

Next, a global analysis of the suitability of the integrity indicators through the complete test scenarios is realized, including the methodology followed in the analysis.

2) Methodology: The methodology followed for the evaluation of the integrity indicators during our experiments can be enumerated as follows.

1) Manually identify the subset of mismatches in the segment assignment in all the circuits: MM/SX, where X stands for the identifier of the scenario.
2) Fix the thresholds for alert for both μLO and LPPL parameters: $\mu\mathrm{LO}_{\mathrm{Th}}$ and $\mathrm{LPPL}_{\mathrm{Th}}$, according to the test used in the training process and the application under consideration. Typical strategies are the minimization of the FAs or MDs, as well as the maximization of the overall performance. To determine good values for the thresholds, it is important that the training test presents a complete set of integrity scenarios.

Authorized licensed use limited to: Universidad de Cartagena. Downloaded on October 20, 2009 at 08:07 from IEEE Xplore. Restrictions apply.

This article has been accepted for inclusion in a future issue of this journal. Content is final as presented, with the exception of pagination.

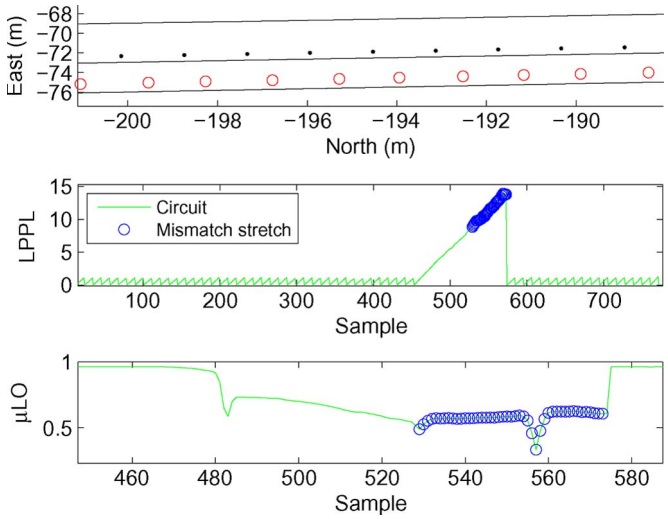

Fig. 10. (Top) Stretch of estimated vehicle trajectory during a mismatch of S3ME. Road lanes (solid black), ground truth (black ·), and filter positions (red o). (Middle) LPPL values along a stretch of the circuit (solid green) and during the period of mismatch (blue o). (Bottom) μLO values along a stretch of the circuit (solid green) and during the period of mismatch (blue o).

3) Determine the subset of samples over (for LPPL) and below (for μLO) the threshold values for every scenario SX: subset $\{\mu\text{LOA/SX}, \text{LPPLA/SX}\}$. Note that $\{\mu\text{LOA/SX}, \text{LPPLA/SX}\}$ may be understood as any combination of both subsets, including not only each subset individually but $\{\mu\text{LOA/SX} \cup \text{LPPLA/SX}\}$ or $\{\mu\text{LOA/SX} \cap \text{LPPLA/SX}\}$ as well. This choice will depend on the intended application.
4) Identify the FAs (FA/SX) when an element of $\{\mu\text{LOA/SX}, \text{LPPLA/SX}\}$ is not contained in MM/SX.
5) Identify the MDs (MD/SX) when an element of MM/SX is not contained in $\{\mu\text{LOA/SX}, \text{LPPLA/SX}\}$.

The FA rate (FAR) and the MD rate (MDR) can be calculated by simply dividing the number of FAs and MDs by the total number of samples in the test. The overall correct detection rate (OCDR) can be calculated as

$$\text{OCDR} = 1 - \text{FAR} - \text{MDR}.$$

For better knowledge of the system performance, different sets were employed to train the system to settle the thresholds and for its evaluation.

3) Performance of Integrity Indicators: In these experiments, as a simple example, we decided to apply somewhat strict system requirements for both integrity parameters and to assume a solution that is valid when it simultaneously verifies both thresholds, i.e., $\{\mu\text{LOA/SX} \cap \text{LPPLA/SX}\}$. The final values were decided based on the MDR, FAR, and OCDR curves of experiment S1ME (see Fig. 11), with the objective of minimizing the MDs, while keeping in mind the possible minimization of FAs. They were finally fixed to $\mu\text{LO}_{\text{Th}} = 0.86$ and $\{\text{LPPL}_{\text{Th}}\} = 1.5$. As can be seen in Fig. 11, these values allow a null rate of MDs. However, observing Fig. 12, we can appreciate that the final OCDR is not the maximum for these values (due to the rate of FAs). Among possible values that minimize the MDR, the one with the best OCDR has been

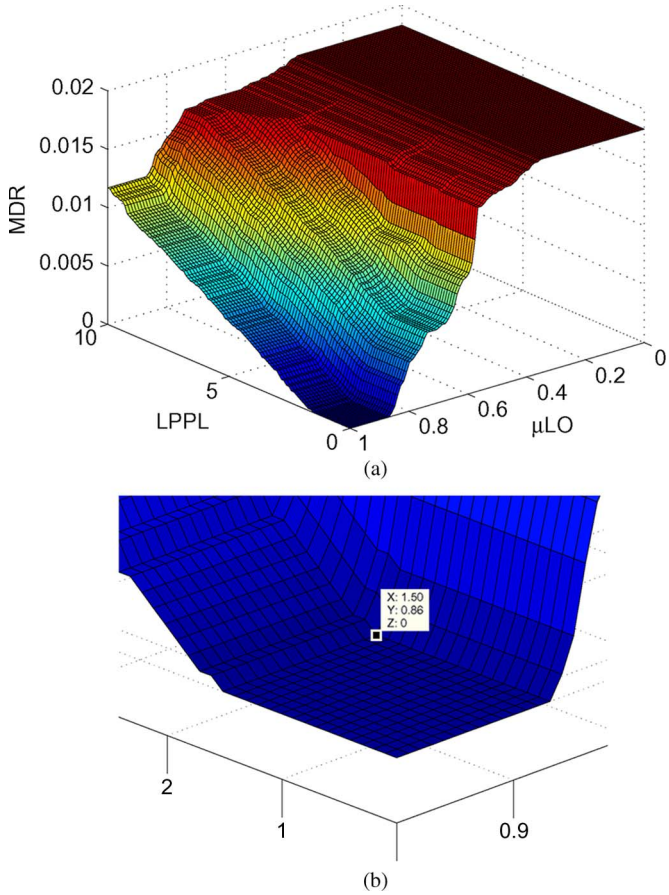

Fig. 11. MDR curves in the experiment of scenario S1ME for threshold values between $\mu\text{LO}_{\text{Th}} \subset \{0, 1\}$ and $\text{LPPL}_{\text{Th}} \subset \{0, 10\}$. (a) Complete curve. (b) Detail of the area with null MDR value and selected thresholds for the analysis.

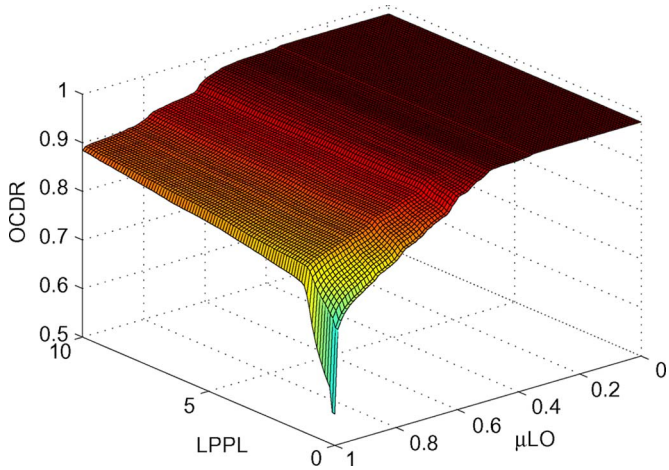

Fig. 12. OCDR curve in the experiment of scenario S1ME for threshold values between $\mu\text{LO}_{\text{Th}} \subset \{0, 1\}$ and $\text{LPPL}_{\text{Th}} \subset \{0, 10\}$.

chosen, offering a final value of OCDR $= 0.8755$. As has been mentioned, the decision of optimizing MDR, FAR, or OCDR depends on the application under consideration.

The goodness of the integrity estimations would depend on their capability to maintain consistent values through all the tests. Table V show the values of interest collected in the experiments realized in the scenarios in Table II. Apart from

Authorized licensed use limited to: Universidad de Cartagena. Downloaded on October 20, 2009 at 08:07 from IEEE Xplore. Restrictions apply.

This article has been accepted for inclusion in a future issue of this journal. Content is final as presented, with the exception of pagination.

TABLE V
INTEGRITY RESULTS FOR DIFFERENT TEST SCENARIOS

Test	MDR	OCDR	FAR	CMR	ECMR
S1E	0.0063	0.9762	0.0175	0.9937	0.9937
S1ME	0.0000	0.8755	0.1245	0.9817	1.0000
S2E	0.0000	0.9921	0.0070	1.0000	1.0000
S2ME	0.0000	0.8522	0.1478	0.9982	1.0000
S3E	0.0119	0.9758	0.0123	0.9873	0.9881
S3ME	0.0012	0.9388	0.0600	0.9803	0.9988

the already-introduced MDR, OCDR, and FAR, we found that it is of interest to include in this table the index of correct match rate (CMR), which represents the rate of correct matches per scenario obtained directly from the lane-assignment process, and the enhanced CMR (ECMR), which stands for the rate of correct matches plus incorrect matches that are correctly identified. Our goal is to obtain values of the ECMR higher than those of the CMR, with the final OCDR being within acceptable limits.

The following conclusions can be yielded by analyzing Table V. The results obtained in the scenario employed in the training process (S1ME) are of the same order as those obtained for the rest of the scenarios. In fact, most of the other five tests used for validation achieved better results in terms of the OCDR, while the value of the ECMR always presents values of unity or very close to unity. This shows the consistency of the indicators. In scenario S1E, there is no difference between the values of the CMR and the ECMR. This is due to the fact that the errors in mismatching are only due to GNSS outliers, which were previously discussed in Section VII-C1. A similar situation appears in scenario S3E. The selection of a high value of $\mu\mathrm{LO}_{\mathrm{Th}}$ and a low value of $\mathrm{LPPL}_{\mathrm{Th}}$ leads to higher rates of FAs, particularly in tests with long GPS gaps. The choice of integrity thresholds always entails a risk, which can be understood as a tradeoff between MDs and FAs.

VIII. COMPUTATIONAL ASPECTS

The algorithm under consideration must be capable of providing real-time integrity and map-matched positions to a road vehicle. For this reason, the computational aspects must be considered in its design. The algorithm was first coded in Matlab and was run using a standard laptop at 1.67 GHz. With both 500 and 1000 particles, the results achieved were very good, and the computational times were under real-time conditions.

Fig. 13 shows further details on the results achieved regarding the computational times. The percentage of the time consumed by the algorithm with respect to the duration of its corresponding test is presented in this figure. The computer employed for the seven experiments was the same standard laptop at 1.67 GHz, and the execution was carried out in Matlab. The number of particles was set to 1000. As can be seen, the computational time rates always show good values. The mean value of these experiments is 54.3, which is enough for the execution of the algorithm, even with a non-time-dedicated software codification. A standard deviation of 2.3 indicates that there are no significant differences among the experiments.

Presently, our team is working on adapting the algorithm to C++ code for its final integration in the prototype vehicle.

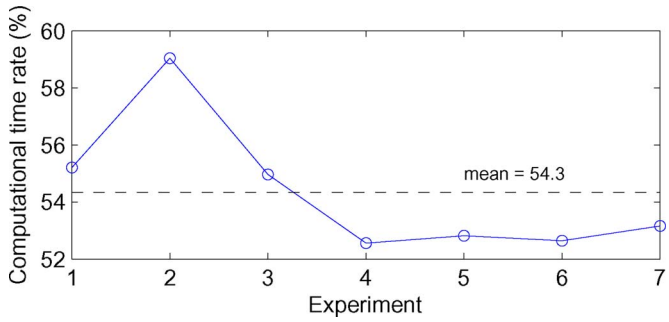

Fig. 13. Computational time rate (execution time divided by the duration of the test) in percentage during the seven experiments with 1000 particles (o). The black dashed line represents the mean value.

IX. CONCLUSION AND FUTURE WORKS

A solution to the problem of integrity in lane-level positioning and map matching has been presented.

A common process for positioning and map matching based on a PF integrates the measurements coming from a GNSS receiver, a gyroscope, and the odometry of the vehicle with the road data stored in an Emap. The information about the geometry and topology of the road at the lane level is employed as an observation for the filtering process. This way, positioning and map matching are provided as a common output, and the vehicle is localized and allocated on the most suitable road lane.

A novel approach for integrity provision of map-matched navigation has been presented. The results achieved show how our method can model the positioning and lane-assignment ambiguities, informing the user when the information coming from the system is not reliable.

Positioning, map-matching, and integrity provision results have been tested in six different scenarios during 30 min of driving, proving the approach's feasibility for lane-level applications.

It was found that, to achieve full integrity in navigation, efficient means for removing GNSS outliers and mitigating multipath effects are highly recommended. The future works of our research group are focused on this issue, along with the preparation of more tests for the validation of the method in very different scenarios such as rural and urban sites.

ACKNOWLEDGMENT

The authors would like to thank M. Schingelhof and his team at the German Aerospace Center (DLR), Institute of Transportation Systems, for their work in the data collection in Berlin.

REFERENCES

[1] D. Obradovic, H. Lenz, and M. Schupfner, "Fusion of sensor data in Siemens car navigation system," *IEEE Trans. Veh. Technol.*, vol. 56, no. 1, pp. 43–50, Jan. 2007.
[2] "SafeSpot European project," Cooperative Vehicles and Road Infrastructure for Road Safety. [Online]. Available: http://www.safespot-eu.org
[3] R. Toledo-Moreo, J. Santa, M. A. Zamora-Izquierdo, B. Bubeda, and A. F. Gomez-Skarmeta, "A study of integrity indicators in outdoor navigation systems for modern road vehicle applications," in *Proc. IROS 2nd Workshop Plan., Perception Navig. Intell. Veh.*, 2008, pp. 9–14.

Authorized licensed use limited to: Universidad de Cartagena. Downloaded on October 20, 2009 at 08:07 from IEEE Xplore. Restrictions apply.

This article has been accepted for inclusion in a future issue of this journal. Content is final as presented, with the exception of pagination.

[4] I. Skog and P. Händel, "In-car positioning and navigation technologies—A survey," *IEEE Trans. Intell. Transp. Syst.*, vol. 10, no. 1, pp. 4–21, Mar. 2009.
[5] T. H. Chang, L. S. Wang, and F.-R. Chang, "A solution to the ill-conditioned GPS positioning problem in an urban environment," *IEEE Trans. Intell. Transp. Syst.*, vol. 10, no. 1, pp. 135–145, Mar. 2009.
[6] C. Goodall and N. El-Sheimy, "The development of a GPS/MEMS INS integrated system utilizing a hybrid processing architecture," in *Proc. ION GNSS*, 2005, pp. 1444–1455.
[7] X. Niu and N. El-Sheimy, "Development of a low-cost MEMS IMU/GPS navigation system for land vehicles using auxiliary velocity updates in the body frame," in *Proc. ION GNSS*, 2005, pp. 2003–2012.
[8] J. Du, J. Masters, and M. Barth, "Lane-level positioning for in-vehicle navigation and automated vehicle location (AVL) systems," in *Proc. IEEE ITSC*, 2004, pp. 35–40.
[9] T. S. Dao, K. Y. K. Leung, C. M. Clark, and J. P. Huissoon, "Co-operative lane-level positioning using Markov localization," in *Proc. IEEE ITSC*, 2006, pp. 1006–1011.
[10] J. Wang, S. Shroedl, K. Mezger, R. Ortloff, A. Joos, and T. Passegger, "Lane keeping based on location technology," *IEEE Trans. Intell. Transp. Syst.*, vol. 6, no. 3, pp. 351–356, Sep. 2005.
[11] R. Toledo-Moreo and M. A Zamora-Izquierdo, "IMM-based lane-change prediction in highways with low-cost GPS/INS," *IEEE Trans. Intell. Transp. Syst.*, vol. 10, no. 1, pp. 180–184, Mar. 2009.
[12] D. Bétaille, R. Toledo-Moreo, and J. Laneurit, "Making an enhanced map for lane location based services," in *Proc. 11th Int. IEEE Conf. Intell. Transp. Syst.*, Beijing, China, Oct. 12–15, 2008, pp. 711–716.
[13] R. Toledo-Moreo, D. Bétaille, F. Peyret, and J. Laneurit, "Fusing GNSS, dead-reckoning and enhanced maps for road vehicle lane-level navigation," *IEEE J. Sel. Topics Signal Process.*, vol. 3, no. 5, Oct. 2009, DOI: 10.1109/JSTSP.2009.2027803.
[14] F. Peyret, D. Bétaille, J. Laneurit, and R. Toledo-Moreo, "Lane-level positioning for cooperative systems using EGNOS and enhanced digital maps," in *Proc. ENC GNSS*, Toulouse, France, Apr. 2008.
[15] R. Toledo-Moreo, M. A. Zamora-Izquierdo, B. Ubeda-Miñarro, and A. F. Gomez-Skarmeta, "High-integrity IMM-EKF-based road vehicle navigation with low-cost GPS/SBAS/INS," *IEEE Trans. Intell. Transp. Syst.*, vol. 8, no. 3, pp. 491–511, Sep. 2007.
[16] E. D. Kaplan, *Understanding GPS: Principles and Applications*. Norwood, MA: Artech House, 1996.
[17] J. Santa, B. Ubeda, R. Toledo-Moreo, and A. F. G. Skarmeta, "Monitoring the position integrity in road transport localization based services," in *Proc. Veh. Technol. Conf.—Fall*, Montreal, QC, Canada, 2006, pp. 1–5.
[18] G. Bacci, F. Principe, M. Luise, C. Terzi, and M. Casucci, "SOFT-REC: A GPS real-time software receiver with EGNOS augmentation," in *Proc. Workshop EGNOS Performance Appl.*, Gdynia, Poland, 2005, pp. 1–7.
[19] O. Le Marchand, P. Bonnifait, J. Ibañez-Guzmán, F. Peyret, and D. Bétaille, "Performance evaluation of fault detection and exclusion algorithms as applied to automotive localisation," in *Proc. Eur. Navig. Conf. GNSS*, Toulouse, France, Apr. 2008.
[20] P. A. Boysen and H. Zunker, "Low cost sensor hybridisation and accuracy estimation for road applications," in *Proc. ESA Conf. Navitec*, Noordwijk, The Netherlands, Dec. 2004.
[21] J. Cosmen-Schortmann, M. Azaola-Sáenz, M. A. Martínez-Olagüe, and M. Toledo-López, "Integrity in urban and road environments and its use in liability critical applications," in *Proc. IEEE Plans Conf.*, 2008, pp. 972–983.
[22] C. A. Scott, "Improved GPS position for motor vehicles through map matching," in *Proc. ION GPS Conf.*, Salt Lake City, UT, 1994.
[23] F. Gustafsson, F. Gunnarsson, N. Bergman, U. Forssell, J. Jansson, R. Karlsson, and P. J. Nordlund, "Particle filters for positioning, navigation, and tracking," *IEEE Trans. Signal Process.*, vol. 50, no. 2, pp. 425–437, Feb. 2002.
[24] K. W. Lee, S. Wijesoma, and J. Ibanez Guzman, "A constrained SLAM approach to robust and accurate localisation of autonomous ground vehicles," *Robot. Auton. Syst.*, vol. 55, no. 7, pp. 527–540, Jul. 2007.
[25] A. N. Cui, L. Hong, and J. R. Layne, "A comparison of nonlinear filtering approaches with an application to ground target tracking," *Signal Process.*, vol. 85, no. 8, pp. 1469–1492, Aug. 2005.
[26] C. Fouque, P. Bonnifait, and D. Bétaille, "Enhancement of global vehicle localization using navigable road maps and dead-reckoning," in *Proc. IEEE Position Location Navig. Syst. Symp.*, Monterey, CA, 2008, pp. 1286–1291.
[27] M. A. Quddus, R. B. Noland, and W. Y. Ochieng, "A high accuracy fuzzy logic-based map-matching algorithm for road transport," *J. Intell. Transp. Syst.*, vol. 10, no. 3, pp. 103–115, 2006.
[28] M. A. Quddus, W. Y. Ochieng, and R. B. Noland, "Current map-matching algorithms for transport applications: State-of-the art and future research directions," *Transp. Res., Part C*, vol. 15, no. 5, pp. 312–328, Oct. 2007.
[29] E. J. Krakiwsky, C. B. Harris, and R. V. C. Wong, "A Kalman filter for integrating dead reckoning, map matching and GPS positioning," in *Proc. IEEE Position Location Navig. Symp.*, Orlando, FL, 1988, pp. 39–46.
[30] M. Yu, Z. Li, Y. Chen, and W. Chen, "Improving integrity and reliability of map matching techniques," *J. Global Positioning Syst.*, vol. 5, no. 1/2, pp. 40–46, 2006.
[31] M. A. Quddus, W. Y. Ochieng, and R. B. Noland, "Integrity of map-matching algorithms," *Transp. Res., Part C*, vol. 14, no. 4, pp. 283–302, Aug. 2006.
[32] Minimum Operational Performance Standards for Global Positioning System/Wide Area Augmentation System Airborne Equipment, Nov. 28, 2001. RTCA, RTCA/DO-229C, Supersedes DO-229B.
[33] Y. Bar-Shalom and X. R. Li, *Estimation and Tracking: Principles, Techniques and Software*. Norwood, MA: Artech House, 1998.

Rafael Toledo-Moreo (M'08) received the M.S. degree in automation and electronics engineering from the Technical University of Cartagena (UPCT), Cartagena, Spain, in 2002 and the Ph.D. degree in computer science from the University of Murcia (UMU), Murcia, Spain, in 2006.

He is an Associate Professor with the Department of Electronics, Computer Technology, and Projects, UPCT. He is also a Research Member of the Intelligent Systems Group, UMU. He has been a Guest Editor of the *International Journal of Intelligent Information and Database Systems*. His main field of interest is road navigation systems.

Dr. Toledo-Moreo is a member of the International Federation of Automatic Control Technical Committee on Transportation Systems and the IEEE Robotics and Automation Society Technical Committee for Intelligent Transportation Systems. He is an Associate Editor and member of the International Program Committees of several conferences related to Intelligent Transportation Systems.

David Bétaille (A'09) received the Ph.D. degree from University College London, London, U.K., in 2004, for his investigations on phase multipath in the kinematic Global Positioning System.

He is a Researcher with the Geolocalization Research Team, Laboratoire Central de Ponts et Chaussees (LCPC), Bouguenais, France, where his current activities relate to vehicle positioning by satellite systems combined with dead reckoning and mapping. Advanced driver-assistance systems and, in general, road-safety applications compose the research context of his laboratory.

François Peyret received the M.S. degree in mechanical engineering from the Ecole Nationale Supérieure de Mécanique et d'Aérotechnique, Poitiers, France, in 1974 and the degree from the École Nationale Supérieure de l'Aéronautique et de l'Espace (SUPAERO), Toulouse, France, in 1975.

He is currently the Director of Research (equivalent of Professor) and the Head of the Image Processing and Geopositioning Research Team, Laboratoire Central de Ponts et Chaussees (LCPC), Bouguenais, France, where he leads research activities in the field of road vehicle positioning for advanced driver-assistance systems particularly hybrid Global Navigation Satellite Systems and enhanced 3-D map matching. His team is currently involved in two major European integrated projects in this field, i.e., CVIS and SAFESPOT from the 3-D eSafety call, as well as several national projects or research actions.

Authorized licensed use limited to: Universidad de Cartagena. Downloaded on October 20, 2009 at 08:07 from IEEE Xplore. Restrictions apply.